Available online at www.sciencedirect.com
ScienceDirect
Journal of Sound and Vibration 311 (2008) 898–911
JOURNAL OF SOUND AND VIBRATION
www.elsevier.com/locate/jsvi

A study of sound shielding control of curved piezoelectric sheets connected to negative capacitance circuits

Hidekazu Kodama*, Munehiro Date, Kohei Yamamoto, Eiichi Fukada

Kobayasi Institute of Physical Research, 3-20-41 Higashi-motomachi, Kokubunji shi, Tokyo 185-0022, Japan

Received 13 January 2007; received in revised form 3 July 2007; accepted 25 September 2007
Available online 31 October 2007

Abstract

A study is conducted on the control of the sound-induced vibrations of a curved piezoelectric composite sheet connected to a negative capacitance circuit. The amplitudes of the sound-induced vibrations of the sheet are measured using a laser Doppler vibrometer. The piezoelectric voltage generated by the sound and the control voltage of the circuit are also measured. When a normal capacitor is used as a circuit element, the vibration of the sheet over a limited frequency band is selectively attenuated by circuit control. The frequency band is controlled by varying the values of the circuit elements. The effective frequency band is increased over a broad frequency range of 40–200 Hz by installing another composite sheet as a capacitor in the circuit. The frequency characteristics of both the ratio of the amplitude of the control voltage of the circuit to that of the piezoelectric voltage of the sheet and the vibration control level of the circuit are expressed as functions of the absolute value of the complex capacitance ratio and the difference between the loss factors of the circuit and the sheet. A vibration amplitude attenuation of up to 27 dB is achieved when the absolute value is matched with the constant depending on the electromechanical coupling factor of the sheet, and the difference between the loss factors is 0.003.

1. Introduction

Electrically shunted piezoelectric materials have been utilized for sound and vibration treatment. It has been noticed that piezoelectric materials connected with passive electrical networks damp the vibrations of structures [1–4]. The possibility of dissipating mechanical energy by using a piezoelectric material shunted with passive electrical circuits has been investigated. It has been shown that shunted piezoelectric elements possess frequency dependent stiffness and loss factor, and shunting with a resistor and inductor introduces an electrical resonance. The frequency of this electrical resonance can be optimally tuned to the structural resonance frequency in a manner analogous to a mechanical vibration absorber.

In the field of sound treatment, sound shielding devices that utilize piezoelectric sheets have the potential to be applied in novel sound shielding technologies. For example, a smart skin that consists of polyvinylidene fluoride (PVDF) films and foams has been mounted in the cockpit of an airplane [5]. This smart skin has demonstrated the potential for reducing interior noise. A distributed parameter sensor made of PVDF film has

*Corresponding author. Tel.: +81 42 321 2841; fax: +81 42 322 4698.
E-mail address: kodama@kobayasi-riken.or.jp (H. Kodama).

0022-460X/$ - see front matter © 2007 Elsevier Ltd. All rights reserved.
doi:10.1016/j.jsv.2007.09.035

also been proposed [6]. This sensor is shaped to measure the acoustic power mode of the total acoustic power radiated from a vibrating plate. By combining this sensor with an adaptive feedforward control, the acoustic power radiated from the vibrating plate is minimized.

A new sound shielding technique that combines a curved piezoelectric sheet and an electric feedback circuit working as a negative capacitor has been proposed [7–9]. The interesting feature of this technique is the combination of a sensor and an actuator into a piezoelectric sheet. In this technique, a piezoelectric sheet is curved to convert its vibration into an in-plane tensile strain. When sound pressure is applied to the sheet, it generates both elastic tensile strain and electric voltage due to the piezoelectric effect. A negative capacitance circuit amplifies the piezoelectric voltage and feeds back the amplified voltage to the sheet. This feedback voltage generates a strain in the sheet because of the inverse piezoelectric effect. The total strain in the sheet is the sum of the sound-induced and voltage-induced strains. Consequently, the apparent elasticity of the sheet is electrically controlled by combining it with a negative capacitance circuit [10]. Additionally, the sound shielding control of a curved PVDF film connected to a negative capacitance has been examined [7]. The sound transmission loss for normal incident sound in the sheet has been measured by using the transfer function method [11,12]. It has been shown that the sound transmission loss of the sheet can be electrically controlled, and it increases up to 40 dB by circuit control. The description and theoretical analysis of the sound shielding characteristics of the curved membranes have been presented [9]. The transmission loss of audible sound passing through the membrane in the system has been expressed as a function of the sound frequency and the geometrical properties of the membrane. It has been shown that the transmission loss of the curved membrane is in proportion to the ratio of the Young's modulus to the square of the radius of curvature of the membrane. It has been theoretically demonstrated that the sound transmission loss of the curved sheet can be increased by changing its Young's modulus. In the field of vibration, the effect of negative capacitance with piezoelectric transducers in damping and absorbing systems has been analyzed. Conventional passive and semi-active configurations of networks have been compared. It has been shown that damping performance has been increased by using a negative capacitance circuit [13].

Recently, a new piezoelectric composite sheet called the macro fiber composite (MFC) sheet has been invented [14,15]. This sheet consists of macro fibers of PZT ceramics with a length of 100 mm and thickness of 0.2 mm and polyimide films printed on a pair of comb-shaped electrodes. The electric dipoles that induce piezoelectricity in the sheet are developed parallel to the fiber. When an in-plane tensile strain is applied to the sheet, a large piezoelectric response is produced due to the d_{33} mode. We have compared the sound shielding control of PVDF with that of MFC. The required voltage amplification of the circuit with MFC, in comparison to that with PVDF, was reduced to 1/20. This is because the electromechanical coupling factor of MFC was five times greater than that of PVDF [16].

The purpose of this paper is to clarify the control characteristics, including frequency response, for negative capacitance circuits connected to piezoelectric materials. Sound-induced vibration is generated on a curved MFC sheet. The vibration control of a negative capacitance circuit is examined. The amplitudes of the sound-induced vibrations are measured using a laser Doppler vibrometer. The electrical properties, i.e., the absolute value of the complex capacitance and the loss factor of the circuit and sheet, are evaluated. The frequency characteristics of both the ratio of the amplitude of the control voltage of the circuit to that of the piezoelectric voltage of the sheet and the vibration control level of the circuit are expressed as functions of the absolute value of the complex capacitance ratio and the difference between the loss factors of the circuit and the sheet.

2. Experimental setup

2.1. Electrical circuits

Fig. 1(a) shows a schematic diagram of the negative capacitance circuit along with the piezoelectric sheet used in this study. A piezoelectric sheet that is subjected to dynamic stress can be modeled as a combination of an electric oscillator and a capacitor C_s. Due to the direct piezoelectric effect, an alternative voltage V_p is generated by the dynamic stress. V_p is measured by connecting a buffer amplifier to a terminal of the sheet, as shown in Fig. 1(b).

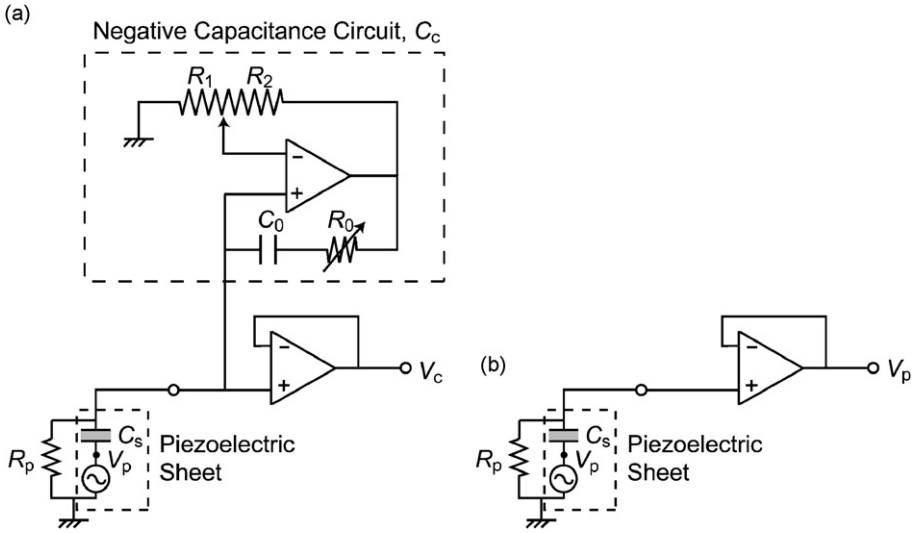

Fig. 1. Schematic circuit diagrams of (a) piezoelectric sheet with a negative capacitance circuit (V_c is the controlling voltage) and (b) piezoelectric sheet without a negative capacitance circuit (V_p is the piezoelectric voltage induced by sound).

As shown in Fig. 1(a), the negative capacitance circuit consists of an operational amplifier (op amp; Burr-Brown OPA-551), a capacitor C_0 and a variable resistor R_0 connected in series, and a resistor split into R_1 and R_2. A piezoelectric sheet connected in parallel with a resistor R_p is connected to the positive input terminal of the op amp. A buffer amplifier is connected to the positive input terminal of the op amp to measure the control voltage V_c of the circuit. The open-loop gain of the op amp is more than 70 dB below 1 kHz.

When the piezoelectric sheet is connected to the circuit, V_p generated by the applied strain causes the flow of electric charge Q from the circuit to the sheet. This charge increases V_c at the positive input terminal of the op amp, and then V_c controls the strain on the sheet.

The relationship between Q and V_c is given as follows:

$$Q = C_c V_c, \tag{1}$$

where C_c is the apparent capacitance of the circuit; the sign of C_c is negative [9].

To study the influence of the dielectric loss of the sheet, the capacitance of the sheet C_s and that of the circuit C_c are treated as complex numbers $C_s^*(= C_s' - iC_s'')$ and $C_c^*(= C_c' - iC_c'')$, respectively. If the voltage amplification of the circuit, which is determined by the ratio of the piezoelectric voltage to the feedback voltage, is sufficiently smaller than the open-loop gain, the frequency characteristics of both the gain and the phase of the op amp can be neglected. C_c^* depends on the values of the various elements as follows:

$$C_c^* = -\frac{R_2}{R_1}\frac{C_0^2}{1+(\omega C_0 R_0)^2}\left(\frac{1}{C_0} - i\omega R_0\right), \tag{2}$$

where ω is the angular frequency.

The absolute value of the capacitance $|C_c^*|$ and the loss factor $\tan\delta_c$ are given as follows:

$$|C_c^*| = \frac{R_2}{R_1}\frac{C_0}{\sqrt{1+(\omega C_0 R_0)^2}}, \tag{3}$$

$$\tan\delta_c = C_c''/C_c' = \omega C_0 R_0. \tag{4}$$

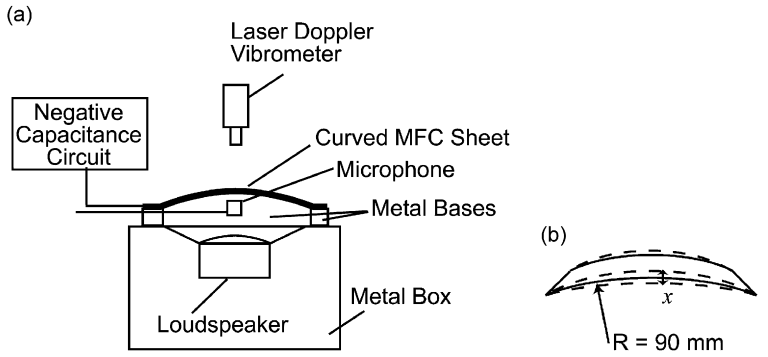

Fig. 2. Depictions of (a) measurement setup and (b) motion of the sheet installed at the setup.

2.2. Setup for vibration measurement

The experimental setup shown in Fig. 2(a) is used to measure the amplitudes of sound-induced vibrations using a laser Doppler vibrometer (Polytech CLV 800 with CLV 1000). An MFC sheet with a length of 110 mm along the fiber direction, width of 75 mm, and thickness of 0.5 mm is used as the sample. The Young's modulus of the sheet is 30.3 GPa. The sheet is connected to the negative capacitance circuit, as shown in Fig. 1(a). A resistor R_p of 6 MΩ is connected in parallel with the sheet to reduce the DC offset voltage applied to it. The sheet is curved along the fiber direction with a radius of curvature of 90 mm and installed at the opening of a chamber made of metal frames. The fundamental resonance frequency of the curved sheet is 6 kHz. The electromechanical coupling factor k of the fixed sheet is 0.265. A loudspeaker placed beneath the sheet generates sound pressure in the chamber. The applied sound pressure level, approximately 100 dB, is measured by a microphone (Rion NL-05) placed inside the chamber. The frequency range of the sound is 40–200 Hz.

As shown in Fig. 2(b), both the ends of the curved sheet are clamped to the metal base to convert its vibration into a uniform in-plane tensile strain on the sheet. The vibration amplitude x of the sheet is measured using a laser Doppler vibrometer. With regard to the sheet, the frequency characteristics of the applied acoustic pressure, x, V_c, and V_p are measured using an FFT analyzer (Rion SA-79).

3. Narrow frequency range control

The frequency characteristics of $|C^*|$ and its loss factor $\tan\delta$ in the sheet and the circuit are shown in Fig. 3. A normal capacitor of 206 nF is used as a circuit element C_0. The values of R_0 and the ratio R_2/R_1 are varied. Here, $|C_s^*|$ and $\tan\delta_s$ are measured using an impedance analyzer (Agilent 4192A), while they are numerically calculated by using Eqs. (3) and (4).

$|C_s^*|$ decreases with an increase in the frequency. Its value is 26 nF at 40 Hz and 24 nF at 200 Hz. $|C_c^*|$ is matched with $C_0(R_2/R_1)$ at 40 Hz, and it then decreases with an increase in the frequency because R_0 is connected in series with C_0. The $\tan\delta_s$ value gradually decreases with the frequency. Its value is 0.18 at 40 Hz and 0.1 at 200 Hz. The $\tan\delta_c$ value is proportional to the frequency and is matched with $\tan\delta_s$ at a single frequency, which increases with a decrease in R_0.

With regard to the sheet, the frequency spectra of the applied sound pressure, V_c, and x are shown in Fig. 4. The voltage V_p generated by the acoustic pressure is plotted against the frequency. The sound pressure decreases with an increase in the frequency. Its value is 2.1 Pa (approximately 100 dB sound level) at 40 Hz and 1.0 Pa (approximately 94 dB) at 200 Hz. V_p is approximately 0.01 V at 40 Hz and it decreases with an increase in the frequency. V_c shows a peak and reaches up to 0.12 V. The frequency at which the voltage is the maximum increases with a decrease in R_0. The vibration amplitude without circuit control, denoted as x_0, decreases with the frequency because of a decrease in the acoustic pressure. The value of the vibration amplitude is 4.2 nm at 40 Hz and 2.4 nm at 200 Hz. The vibration amplitude with circuit control shows a minimum and decreases to 0.2 nm.

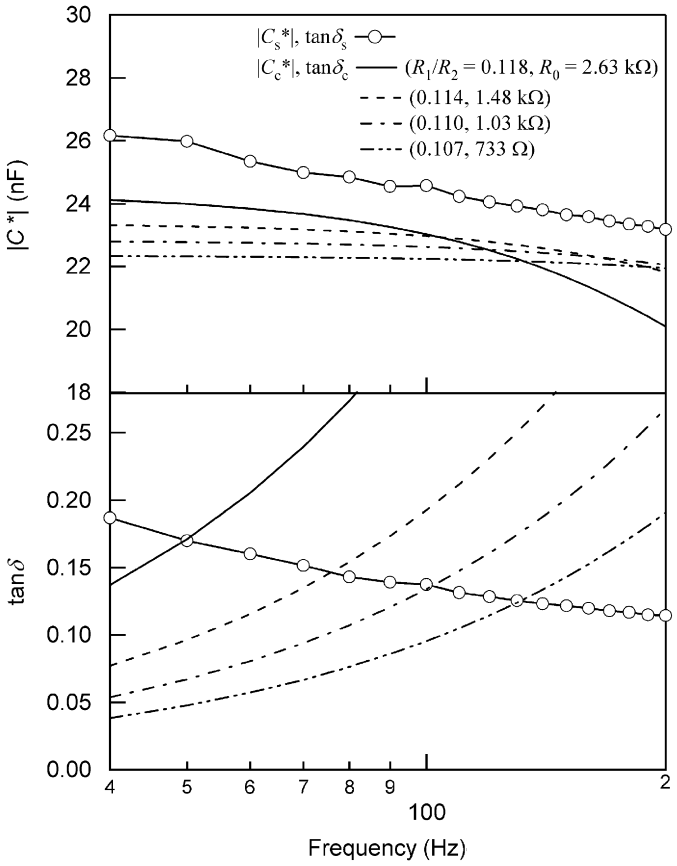

Fig. 3. Frequency spectra of the absolute value $|C^*|$ of the complex capacitance and the loss factor $\tan\delta$ of the sheet ($|C_s^*|$, $\tan\delta_s$) and those of the circuit in which a normal capacitor is installed ($|C_c^*|$, $\tan\delta_c$).

Table 1 shows a comparison of R_0, $f_{\tan\delta_c=\tan\delta_s}$, and $f_{\text{minimum vibration}}$. Here, $f_{\tan\delta_c=\tan\delta_s}$ is the frequency at which $\tan\delta_c = \tan\delta_s$, and $f_{\text{minimum vibration}}$ is the frequency at which the vibration amplitude is minimum. These results clearly indicate that the vibration amplitude shows a minimum at the frequency defined by $\tan\delta_c = \tan\delta_s$. This implies that if $\tan\delta_s$ is known, this frequency can be chosen by the appropriate C_0 and R_0.

The above-mentioned data indicate that the vibration amplitude over a limited frequency range is selectively reduced by circuit control; therefore, the controllable frequency range can be changed by varying R_0. By comparing the frequency spectra of $\tan\delta_c$ and $\tan\delta_s$ shown in Fig. 3, it is noticed that V_c shows a maximum and the vibration amplitude shows a minimum when $\tan\delta_c$ is matched with $\tan\delta_s$.

4. Wide frequency range control

To increase the controllable frequency range of the circuit, another MFC sheet is used as the circuit element C_0. Because the loss factor of the normal capacitor is negligible, its capacitance is treated as a real number. Here, C_0 should be treated as a complex number $C_0^*(= C_0' - iC_0'')$. From Eq. (2), it is estimated that the loss factor of the circuit is matched with that of the sheet over a broad frequency range when the same sheet is used as a capacitor in the circuit.

A comparison between the $|C^*|$ and $\tan\delta$ values obtained from the experimental data for the sheet and those obtained from numerically calculated data of the improved circuit is shown in Fig. 5. A resistance of 2.6 kΩ is used as R_0 in order to attenuate high-frequency oscillations. The value of R_2/R_1 is 0.93.

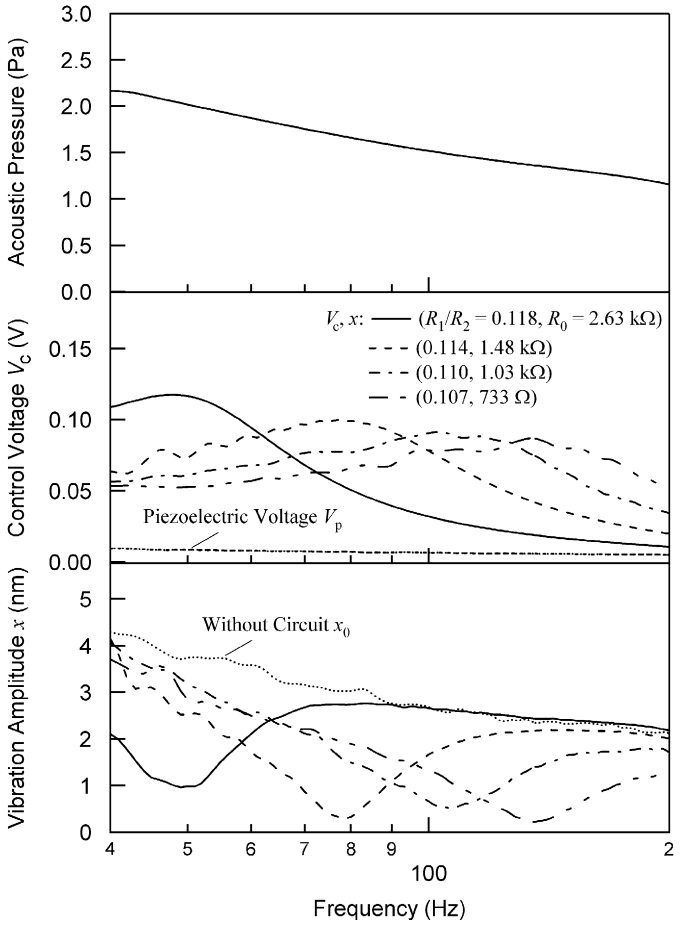

Fig. 4. Frequency spectra of the applied acoustic pressure, V_c (V_p is represented by the dotted line), and the vibration amplitude of the sheet without control x_0 (dotted line) and with control x for the circuit in which a normal capacitor is installed as C_0.

Table 1
Comparison of R_0, $f_{\tan\delta_c=\tan\delta_s}$, and $f_{\text{minimum vibration}}$

R_0 (Ω)	$f_{\tan\delta_c=\tan\delta_s}$ (Hz)	$f_{\text{minimum vibration}}$ (Hz)
2630	50	50
1480	75	78
1030	100	105
733	130	135

In comparison with the case shown in Fig. 3 for the circuit in which the normal capacitor is installed, $|C_c^*|$ and $\tan\delta_c$ in the improved circuit are nearly constant. $|C_c^*|$ is approximately 0.93 times $|C_s^*|$ over a broad frequency range 40–200 Hz. The $\tan\delta_c$ value is approximately 0.15 and is matched with $\tan\delta_s$ at 75 Hz. Below this frequency, $\tan\delta_c$ is smaller than $\tan\delta_s$ because of the resistor R_p connected in parallel with the sheet. Above this frequency, $\tan\delta_c$ is larger than $\tan\delta_s$ because of the resistor R_0 connected in series with the MFC capacitor in the circuit.

With regard to the improved circuitry, the plots shown in Fig. 6 are the same as those shown in Fig. 4. V_c decreases with an increase in the frequency. The results correspond with those for the frequency spectrum of the acoustic pressure. The voltage is 0.13 V at 40 Hz and 0.06 V at 200 Hz. It is remarkable

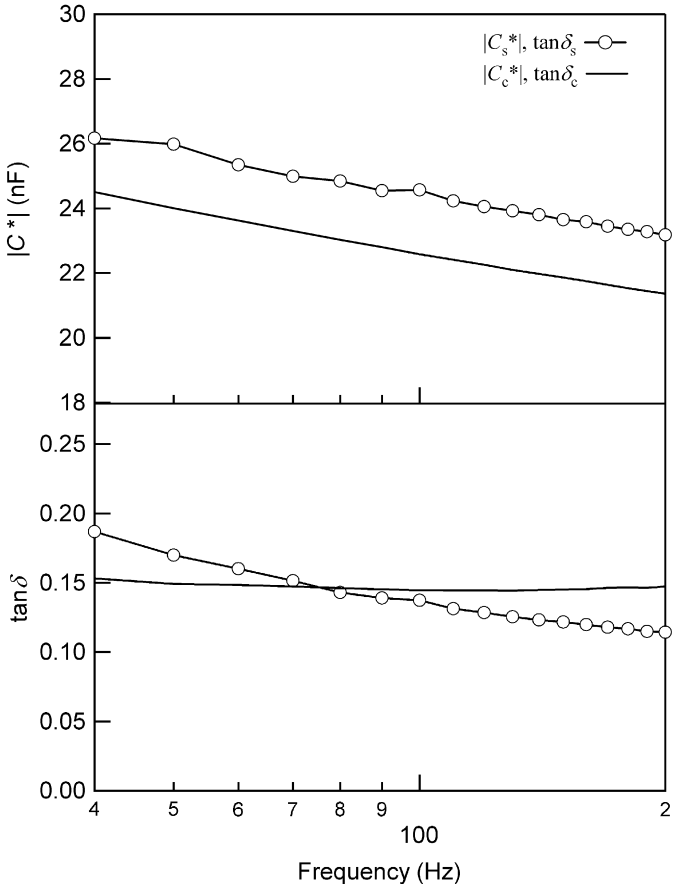

Fig. 5. Frequency spectra of $|C^*|$ and $\tan\delta$ for the sheet ($|C_s^*|$, $\tan\delta_s$) and those for the circuit in which the MFC capacitor is installed as C_0 ($|C_c^*|$, $\tan\delta_c$).

that the vibration amplitudes decrease over a broad frequency range of 40–200 Hz when only C_0 is replaced with the MFC capacitor in the circuit. The minimum vibration amplitude is 0.1 nm at approximately 100 Hz.

5. Vibration control characteristics of negative capacitance circuits

5.1. Frequency characteristics

It has been reported that the Young's modulus Y of a piezoelectric sheet connected to a negative capacitance circuit is expressed as a function of C_c/C_s as follows:

$$Y = Y^E\left(1 - \frac{k^2}{1 + C_c/C_s}\right)^{-1}, \tag{5}$$

where Y^E is the Young's modulus in a constant electric field, and k is the electromechanical coupling factor of the sheet [10]. In this study, the capacitance ratio is treated as a complex number. The ratio of the complex capacitance of the circuit to that of the sheet is given by

$$\frac{C_c^*}{C_s^*} = \frac{C_c'(1 - \mathrm{i}\tan\delta_c)}{C_s'(1 - \mathrm{i}\tan\delta_s)} = \frac{C_c'\{(1 - \tan\delta_c\tan\delta_s - \mathrm{i}(\tan\delta_c - \tan\delta_s)\}}{C_s'(1 + \tan^2\delta_s)}. \tag{6}$$

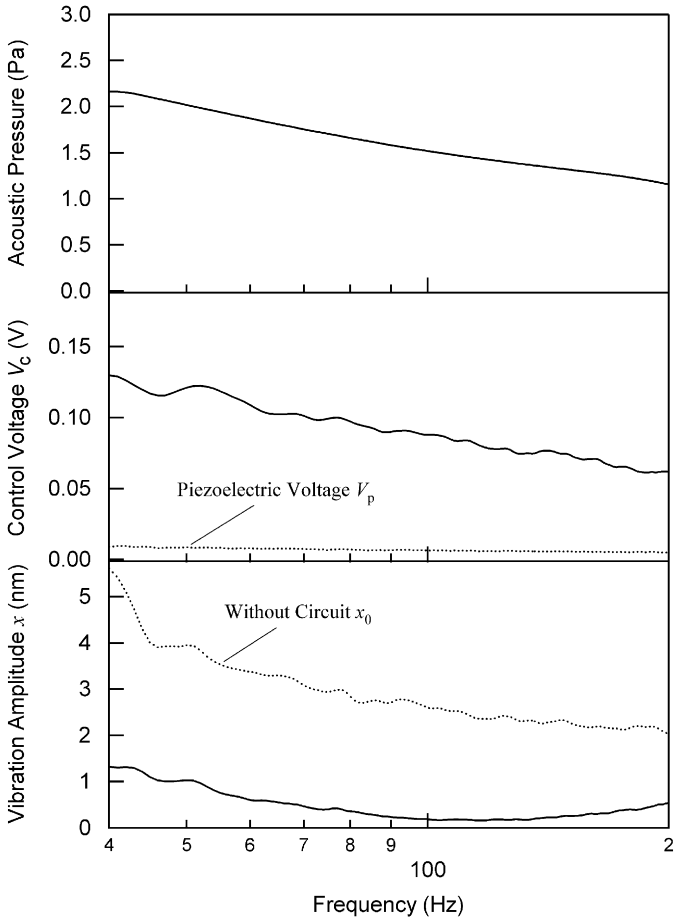

Fig. 6. Frequency spectra of the applied acoustic pressure, V_c (V_p is represented by the dotted line), and x_0 (dotted line) and x for the circuit in which an MFC capacitor is installed as C_0.

Because the square of $\tan\delta_s$ and the product $\tan\delta_s \tan\delta_c$ are considerably smaller than 1, $1+\tan\delta_s^2$ and $1+\tan\delta_c \tan\delta_s$ are assumed to be 1. Eq. (6) is simplified as follows:

$$\frac{C_c^*}{C_s^*} \approx \frac{C_c'}{C_s'}\{(1 - i(\tan\delta_c - \tan\delta_s)\}. \tag{7}$$

Furthermore, the square of $\tan\delta_c - \tan\delta_s$ is considerably smaller than 1. Thus, the simplified equation for the absolute value of the ratio $|C_c^*/C_s^*|$ is given as follows:

$$-\left|\frac{C_c^*}{C_s^*}\right| \approx \frac{C_c'}{C_s'}. \tag{8}$$

In this equation, the minus sign of the left-hand side term implies that C_c^* is a negative capacitance. From Eqs. (5), (7), and (8), we can derive a simplified equation showing the relationship between Y and the ratio of the complex capacitance as follows:

$$Y = Y^E\left[1 - \frac{k^2}{1 - |C_c^*/C_s^*|\{(1 - i(\tan\delta_c - \tan\delta_s)\}}\right]^{-1}. \tag{9}$$

This equation implies that the Young's modulus depends on not only the absolute value of the ratio $|C_c^*/C_s^*|$, but also the difference between the loss factors, $\tan\delta_c - \tan\delta_s$. The equation also implies that the Young's modulus is divergent when $|C_c^*/C_s^*| = 1 - k^2$ and $\tan\delta_c - \tan\delta_s = 0$.

On the basis of the experimental data shown in Fig. 3, both $|C_c^*/C_s^*|$ and $\tan\delta_c - \tan\delta_s$ are calculated for the case of the sheet with the circuit in which the normal capacitor is installed. Fig. 7 shows the frequency spectra of $|C_c^*/C_s^*|$ and $\tan\delta_c - \tan\delta_s$. The dashed lines represent $|C_c^*/C_s^*| = 1 - k^2 = 0.93$ and $\tan\delta_c - \tan\delta_s = 0$. The absolute value shows a broad peak; then, the frequency at which the absolute value shows a maximum increases with a decrease in R_0. The difference between the loss factors increases with a decrease in the frequency and becomes zero, i.e., $\tan\delta_c$ is matched with $\tan\delta_s$ at a single frequency. The frequency at which the difference between the loss factors becomes 0 increases with a decrease in R_0.

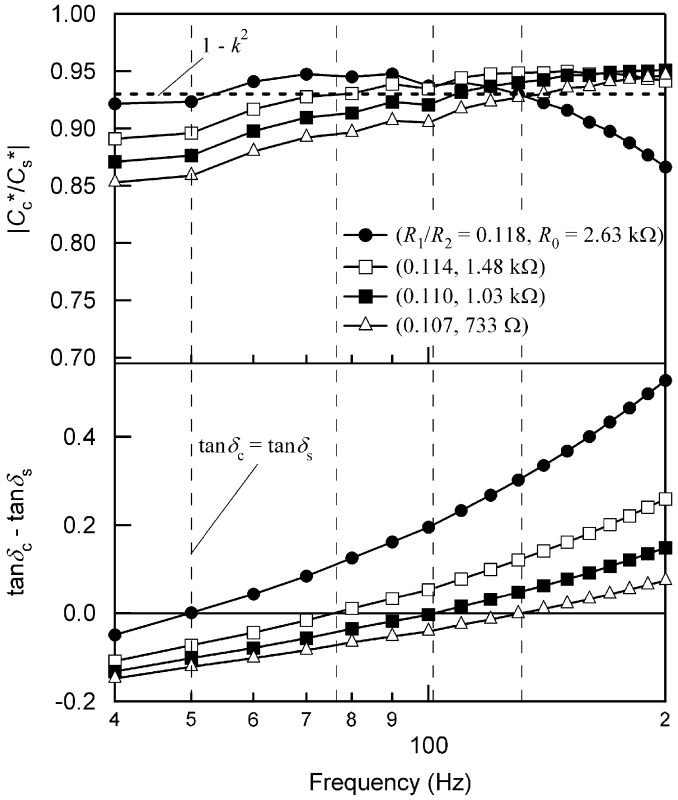

Fig. 7. Frequency spectra of $|C_c^*/C_s^*|$ and $\tan\delta_c - \tan\delta_s$ in the sheet connected to the circuit in which a normal capacitor is installed as C_0.

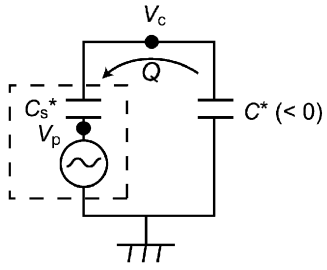

Fig. 8. Equivalent circuit of a piezoelectric sheet connected to a negative capacitance circuit.

Fig. 8 shows the simplified equivalent circuit of the piezoelectric sheet connected to the negative capacitance circuit. The sheet is modeled as a capacitor C_s^* with a voltage generator. The negative capacitance circuit is modeled as a capacitor C_c^*. Here, V_c corresponds to the voltage of the point between the sheet and the circuit. The absolute value of the voltage ratio $|V_c/V_p|$, where V_p is the piezoelectric voltage, depends on the ratio of the capacitances C_c^*/C_s^*. From this relationship and Eqs. (7) and (8), the voltage ratio is given as follows:

$$|V_c/V_p| = \left|\frac{1}{1+C_c^*/C_s^*}\right| = \left|\frac{1}{1-\left|C_c^*/C_s^*\right|\{(1-\mathrm{i}(\tan\delta_c-\tan\delta_s)\}}\right| = \frac{1}{\sqrt{\left(1-\left|C_c^*/C_s^*\right|\right)^2+\left|C_c^*/C_s^*\right|^2(\tan\delta_c-\tan\delta_s)^2}}. \quad (10)$$

The amplitude of the vibration caused by the in-plane tensile strain depends on the inverse of the Young's modulus of the sheet [10]. From Eq. (9), the relationship between the absolute value of the vibration amplitude ratio $|x/x_0|$, where x_0 is the vibration amplitude without circuit control, and C_c^*/C_s^* is given as follows:

$$|x/x_0| = \left|1-\frac{k^2}{1-\left|C_c^*/C_s^*\right|\{(1-\mathrm{i}(\tan\delta_c-\tan\delta_s)\}}\right| = \frac{\sqrt{\{(1-\alpha-k^2)(1-\alpha)+\alpha^2\beta^2\}^2+k^4\alpha^2\beta^2}}{(1-\alpha)^2+\alpha^2\beta^2}, \quad (11)$$

where $\alpha = |C_c^*/C_s^*|$, $\beta = \tan\delta_c - \tan\delta_s$.

In this study, as shown in Eqs. (10) and (11), both $|V_c/V_p|$ and $|x/x_0|$ can be expressed as simplified functions of $|C_c^*/C_s^*|$ and $\tan\delta_c - \tan\delta_s$ as opposed to conventional equations where the ratios are expressed in terms of real number values of C_c and C_s in Date's model [10].

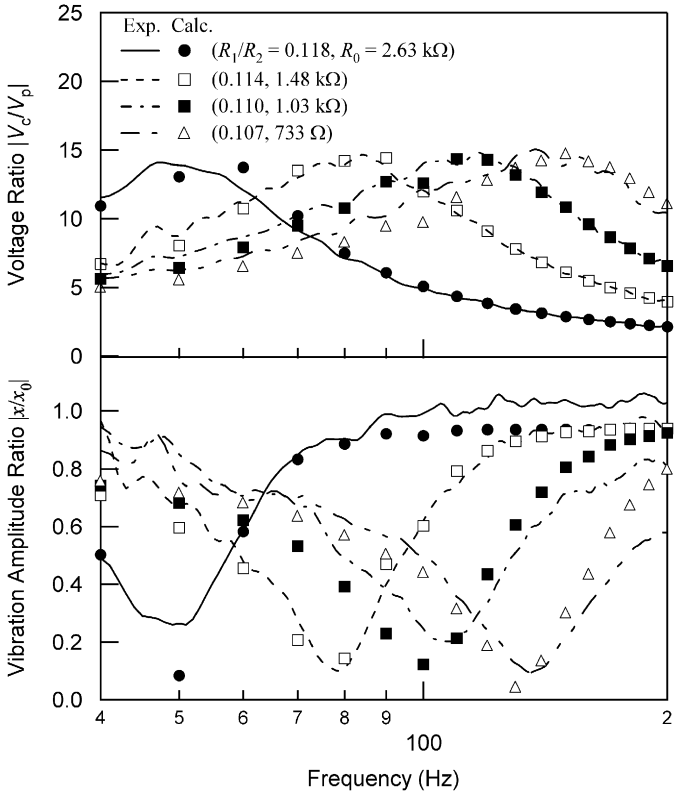

Fig. 9. Experimental and calculated data of the frequency spectra of the voltage ratio $|V_c/V_p|$ and the vibration amplitude ratio $|x/x_0|$ in the sheet for the circuit in which a normal capacitor is installed as C_0.

Fig. 9 shows a comparison between the data derived from the experimental results in Fig. 4 and the numerically calculated data obtained from Eqs. (10) and (11) with respect to $|V_c/V_p|$ and $|x/x_0|$. In both cases, it is remarkable that the experimental data are in good agreement with the numerically calculated data. In the case of the vibration amplitude ratio, the differences between the experimental data and estimated data are caused by the extremely small values of the vibration amplitude—less than 5 nm—due to the large elasticity of the curved sheet. The $|V_c/V_p|$ value shows a peak and its maximum value is approximately 15, i.e., 23 dB. The $|x/x_0|$ value shows a minimum and decreases to 0.1. In comparison with the frequency spectra of $|V_c/V_p|$, those of $|x/x_0|$ are sensitive to variations in the frequency.

In the case of $R_0 = 2.63\,\mathrm{k\Omega}$ and $R_2/R_1 = 0.118$, as shown in Figs. 7 and 9, $|C_c^*/C_s^*| = 0.923$ at 50 and 140 Hz. When the difference between the loss factors is omitted, both $|V_c/V_p|$ and $|x/x_0|$ depend on only $|C_c^*/C_s^*|$. In this case, $|V_c/V_p| = 13.0$ and $|x/x_0| = 0.09$ when $|C_c^*/C_s^*| = 0.923$. However, the results show that $|V_c/V_p| = 13.0$ and 3.1 and $|x/x_0| = 0.09$ and 0.97 at 50 and 140 Hz, respectively. The results indicate that the values of $\tan\delta_c - \tan\delta_s$, that is, 0.001 at 50 Hz and 0.335 at 140 Hz, obviously reduce both $|V_c/V_p|$ and the vibration control efficiency of the circuit.

The results for the values of $|C_c^*/C_s^*|$ and $\tan\delta_c - \tan\delta_s$ in the sheet for the circuit in which an MFC sheet is installed as a capacitor C_0 are shown in Fig. 10. In comparison with the case of the circuit in which the normal capacitor is installed, as shown in Fig. 7, $|C_c^*/C_s^*|$ is nearly constant and $\tan\delta_c - \tan\delta_s$ slightly increases with the frequency. It is noticed that the absolute value is matched with $1-k^2 = 0.93$ over a broad frequency range of 40–200 Hz and $\tan\delta_c - \tan\delta_s$ reduces to below 1/10 of the value in the case of the circuit in which the normal capacitor is installed.

Fig. 11 shows the same plots as those shown in Fig. 9 for the circuit in which the MFC sheet is installed as the capacitor. The results show that the estimated data obtained by using Eqs. (10) and (11) are in good agreement with the data calculated from the experimental data shown in Fig. 6. The $|V_c/V_p|$ value is approximately 14 and it gradually decreases with the frequency. The $|x/x_0|$ value decreases to below 0.3 over a

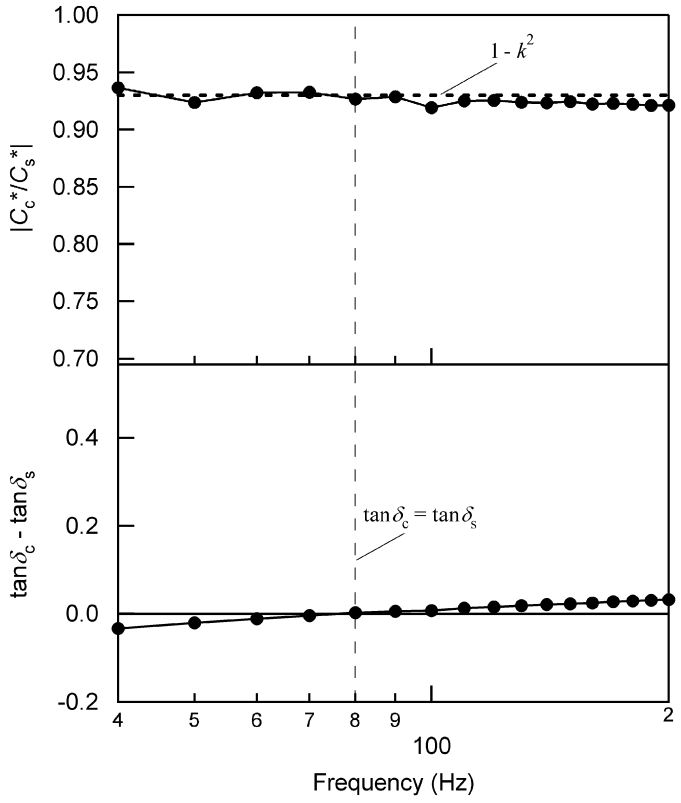

Fig. 10. Frequency spectra of $|C_c^*/C_s^*|$ and $\tan\delta_c - \tan\delta_s$ in the sheet connected to the circuit in which the MFC capacitor is installed as C_0.

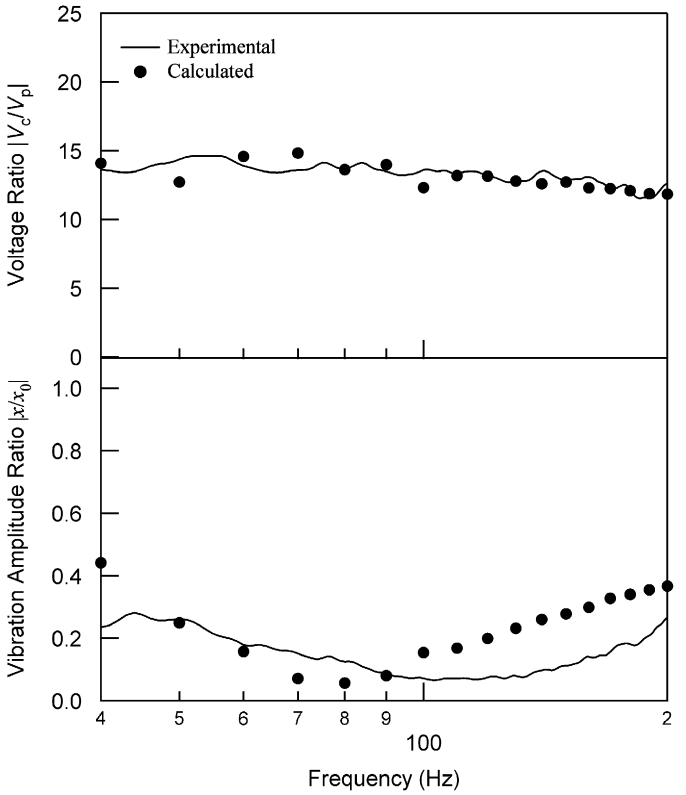

Fig. 11. Experimental and calculated data of the frequency spectra of $|V_c/V_p|$ and $|x/x_0|$ in the sheet for the circuit in which the MFC capacitor is installed as C_0.

broad frequency range of 40–200 Hz. In this study, the vibration amplitudes are 3–5 nm without circuit control, and they reduce to less than 1 nm by circuit control. The discrepancy between the predicted and measured results is caused by such a small value, which is close to the measurement limit of the measurement equipment. However, the results shown in Figs. 10 and 11 indicate that $\tan\delta_c - \tan\delta_s$ is minimized over a broad frequency range and the controllable frequency range is increased by installing an MFC sheet as a capacitor in the circuit.

5.2. Vibration control level

The plots of the attenuation level of the vibration amplitude on a dB scale and the change in the Young's modulus Y/Y^E against $|C_c^*/C_s^*|$ are shown in Fig. 12. The attenuation level is given by $-10\log_{10}|x/x_0|^2$. The vibrations of the sheet are generated by a single-frequency sound. The value of R_0 in the circuit is varied to match the loss factor of the circuit with that of the sheet, and the resistance ratio R_2/R_1 is controlled to change $|C_c^*/C_s^*|$.

The attenuation level appears to increase with a decrease in $|C_c^*/C_s^*|$ and reaches 27 dB of attenuation at $|C_c^*/C_s^*| = -0.93$. Below this value of the ratio, the level decreases because of the excessive strain generated by the control voltage of the circuit. The sign of the level changes to negative below $|C_c^*/C_s^*| = -0.96$. This implies that negative elasticity is realized by circuit control. This result also indicates that the Young's modulus increases by 25 times and becomes 757.5 GPa.

The numerically calculated data obtained by using Eq. (11) are in good agreement with the experimental data when $k = 0.265$ and $\tan\delta_c - \tan\delta_s = 0.003$. The results reveal that the maximum vibration attenuation level is 27 dB at $|C_c^*/C_s^*| = 1 - k^2 = 0.93$ and $\tan\delta_c - \tan\delta_s = 0.003$. The $\tan\delta_s$ value is approximately 0.15 in

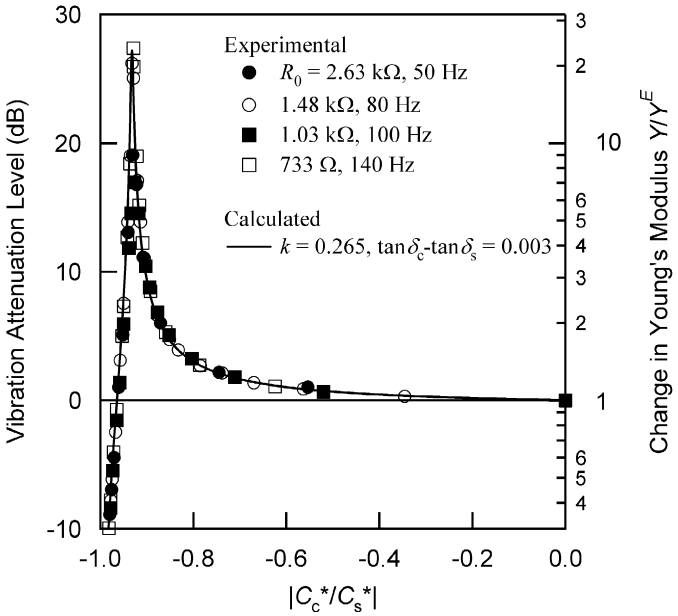

Fig. 12. Plots of the vibration attenuation levels and change in the Young's modulus Y/Y^E against the $|C_c^*/C_s^*|$ values obtained from experimental data and calculated data of Eq. (11) with $k = 0.265$ and $\tan\delta_c - \tan\delta_s = 0.003$.

the measured frequency range. The experimental data reveal that a difference of approximately 2% between the loss factors of the circuit and the sheet has been achieved, thereby resulting in a 27 dB reduction in the vibration amplitude of the sheet.

6. Conclusions

In this study, a novel sound-shielding device comprising a curved MFC sheet and negative capacitance circuits is proposed. We have closely examined the sound shielding control properties of the negative capacitance circuits with the curved MFC sheet. The experimental results show that the effective frequency band is limited when a normal capacitor is used. The effective frequency band is broadened by using the MFC sheet as a capacitor in the circuit.

The ratio of the control voltage of the circuit to the piezoelectric voltage of the sheet and the vibration control level of the circuit are expressed as simplified functions of parameters such as the absolute value of the complex capacitance ratio $|C_c^*/C_s^*|$ and the difference of the loss factors $\tan\delta_c - \tan\delta_s$ of the circuit and the sheet. In this study, we have shown that the experimental data are in good agreement with the data estimated by these equations.

In this study, a vibration amplitude attenuation of up to 27 dB is achieved under conditions in which $|C_c^*/C_s^*|$ is matched with $1-k^2$ and $\tan\delta_c - \tan\delta_s = 0.003$. By introducing computer control techniques, the difference between the loss factors could become smaller than the value obtained in the present study and the maximum vibration attenuation level will increase further. Nevertheless, we have presented a detailed analysis on the control of the circuit including the frequency characteristics. This study enables us to easily estimate and design the sound shielding control characteristics of curved piezoelectric sheets with negative capacitance circuits.

Acknowledgment

This study was supported by a grant-in-aid for scientific research from the Japan Society for the Promotion of Science.

References

[1] R.L. Forward, Electronic damping of vibrations in optical structures, *Journal of Applied Optics* 18 (1979) 690–697.

[2] N.W. Hagood, A. von Flotow, Damping of structural vibrations with piezoelectric materials and passive electrical networks, *Journal of Sound and Vibration* 146 (1991) 243–268.

[3] S.O.R. Moheimani, A survey of recent innovations in vibration damping and control using shunted piezoelectric transducers, *IEEE Transactions on Control Systems Technology* 11 (2003) 482–494.

[4] C.M.A. Vasques, J.D. Rodrigues, Active vibration control of a smart beam through piezoelectric actuation and laser vibrometer sensing: simulation, design and experimental implementation, *Smart Materials and Structures* 16 (2007) 305–316.

[5] C. Guigou, C.R. Fuller, Control of air craft interior broadband noise with foam-PVDF smart skin, *Journal of Sound and Vibration* 220 (1999) 541–557.

[6] N. Tanaka, Y. Kikushima, M. Kuroda, S.D. Snyder, Active control of acoustic power radiated from a vibrating planar structure using smart sensors, *JSME International Journal* 39 (1996) 49–57.

[7] E. Fukada, M. Date, K. Kimura, T. Okubo, H. Kodama, P. Mokry, K. Yamamoto, Sound isolation by piezoelectric polymer films connected to negative capacitance circuit, *IEEE Transactions on Dielectrics and Electrical Insulation* 11 (2004) 328–333.

[8] E. Fukada, M. Date, H. Kodama, Y. Oikawa, Elasticity control of curved piezoelectric polymer films, *Ferroelectrics* 320 (2005) 3–13.

[9] P. Mokry, E. Fukada, K. Yamamoto, Noise shielding system utilizing a thin piezoelectric membrane and elasticity control, *Journal of Applied Physics* 94 (2003) 789–796.

[10] M. Date, M. Kutani, S. Sakai, Electrically controlled elasticity utilizing piezoelectric coupling, *Journal of Applied Physics* 87 (2000) 863–868.

[11] J.Y. Chung, D.A. Blaser, Transfer function method of measuring in-duct acoustic properties. I. Theory, *Journal of Acoustical Society of America* 68 (1980) 907–913.

[12] J.Y. Chung, D.A. Blaser, Transfer function method of measuring in-duct acoustic properties. II. Experiment, *Journal of Acoustical Society of America* 68 (1980) 914–921.

[13] M. Neubauer, R. Oleskiewicz, K. Poop, T. Kryzynski, Optimization of damping and absorbing performance of shunted piezo elements utilizing negative capacitance, *Journal of Sound and Vibration* 298 (2006) 84–107.

[14] W.K. Wilkie, R.G. Bryant, J.W. High, R.L. Fox, R.F. Hellbaum, A. Jalink, B.D. Little, P.H. Mirick, Low-cost piezocomposite actuator for structural control applications, *Proceedings of Seventh SPIE International Symposium on Smart Structure and Materials*, Newport Beach, CA, March 5–9, 2000.

[15] H.A. Sodano, G. Park, D.J. Inman, An investigation into the performance of macro-fiber composite for sensing and structural vibration applications, *Mechanical Systems and Signal Processing* 18 (2004) 683–697.

[16] H. Kodama, K. Yamamoto, M. Date, E. Fukada, Vibration control of curved piezoelectric sheets using negative capacitance circuits, *Ferroelectrics* 351 (2007) 33–42.